


Radio-Frequency Magnetometry Based on Parametric Resonances

Wei Xiao^{1,2,3}, Xiyu Liu¹, Teng Wu^{1,*}, Xiang Peng¹, and Hong Guo^{1,†}

¹State Key Laboratory of Advanced Optical Communication Systems and Networks, School of Electronics, and Center for Quantum Information Technology, Peking University, Beijing 100871, China

²MIT Key Laboratory of Complex-field Intelligent Sensing, Advanced Research Institute of Multidisciplinary Science, Beijing Institute of Technology, Beijing 100081, China

³State Key Laboratory of CNS/ATM, Beijing Institute of Technology, Beijing 100081, China

 (Received 29 April 2024; revised 21 June 2024; accepted 31 July 2024; published 27 August 2024)

We propose and demonstrate a radio-frequency (rf) atomic magnetometer based on parametric resonances. Previously, most rf atomic magnetometers are based on magnetic resonances and their sensitivities are often limited by spin-exchange relaxation. Here, we introduce a novel scheme for an rf magnetometer where the rf magnetic field is measured by exciting the parametric resonances instead of magnetic resonances using parametric modulation fields. In this way, the spin-exchange relaxation is almost eliminated. Benefiting from the low spin relaxation rate, the parametric resonance scheme exhibits a narrower linewidth and stronger signal, which results in a higher sensitivity. With a $6 \times 6 \times 3 \text{ mm}^3$ Rb atomic vapor cell, we developed an rf atomic magnetometer with a noise floor of $2 \text{ fT/Hz}^{1/2}$, which is about one order of magnitude higher than the sensitivity achieved in the magnetic-resonance-based scheme. The presented rf detection scheme holds promise in advancing rf atomic magnetometers and brings new insight into their various applications.

DOI: [10.1103/PhysRevLett.133.093201](https://doi.org/10.1103/PhysRevLett.133.093201)

Introduction—As one of the fundamental and observable physical quantities, the fast-oscillating magnetic field detection is of great interest across various applications. Among different types of radio-frequency (rf) magnetometers that aims to detect oscillating magnetic fields in the rf range [1–4], the atomic magnetometer stands out for their exceptional sensitivity, achieving sub-fT/Hz^{1/2} noise floors [5–7]. Additionally, the atomic magnetometer further offers advantages such as low running cost, potential for miniaturization, and a broad operating frequency range with a flat response. Benefiting from these features, it has proved to be a powerful tool in various fields, such as magnetic induction tomography (MIT) [8–13], nuclear magnetic resonance (NMR) [14–18], magnetic resonance imaging (MRI) [19–23], and nuclear quadrupole resonance [5,24–26].

The rf atomic magnetometer typically relies on the detection of magnetic resonance (MR) signals by applying a static bias field B_0 to tune the Zeeman splitting of atoms. When a transverse rf field with a frequency matching the Zeeman splitting of adjacent sublevels is applied, the magnetic resonance emerges [27] and the information of the rf field can be extracted. While widely successful, these magnetometers encounter challenges associated with spin-exchange (SE) relaxation [28–30], a dominant mechanism that broadens MR signals and

diminishes sensitivity, particularly in buffer-gas-filled atomic vapor cells [5–7,15,25,31,32].

Although the SE relaxation can be completely eliminated by operating near zero magnetic field, as in a spin-exchange relaxation-free (SERF) magnetometer [33,34], the MR-based rf atomic magnetometer requires a large bias field that conflicts with the SERF condition. There are many efforts have been made to suppress the SE relaxation, such as operating the rf atomic magnetometer in antirelaxation coated atomic vapor cells [12,35,36], using pulse magnetic fields to cancel the bias field [37], and employing light narrowing effects [38,39]. Among these methods, the light narrowing effect, which requires only high polarization of atoms, is a common choice to suppress the SE relaxation instead. However, to fully polarize the atomic ensemble, a strong polarized light is required to perform the optical pumping, which would lead to extra spin relaxation caused by power broadening of the pump light [40].

In addressing these challenges, we propose and experimentally demonstrate a novel scheme based on parametric resonances (PR) rather than MR to realize an rf atomic magnetometer, eliminating the need for a static bias field. By utilizing longitudinal parametric resonances with pulse modulations, the SE relaxation is further suppressed, and the sensitivity of rf atomic magnetometer is improved by an order of magnitude compared to conventional schemes. We achieve a remarkable noise floor of $\sim 2 \text{ fT/Hz}^{1/2}$ within a small $6 \times 6 \times 3 \text{ mm}^3$ ⁸⁷Rb atomic vapor cell. A theoretical model is also developed to analytically demonstrate the principle of the scheme.

*Contact author: wuteng@pku.edu.cn

†Contact author: hongguo@pku.edu.cn

Theoretical model—The dynamic evolution of the ground-state electron spin polarization \mathbf{P} under the effects of magnetic field \mathbf{B} can be approximately described by the Bloch equation

$$\frac{d}{dt}\mathbf{P} = \gamma\mathbf{P} \times \mathbf{B} + R_{\text{OP}}(\mathbf{s} - \mathbf{P}) - \Gamma_0\mathbf{P}, \quad (1)$$

where γ is the gyromagnetic ratio, R_{OP} is the optical pumping rate, \mathbf{s} is the optical pumping vector, and Γ_0 is the phenomenological spin relaxation rate. To demonstrate the basic principle of the PR-based rf field detection scheme, we consider a case that there is a rotating magnetic field $\mathbf{B}_m = \hat{x}B_m \sin \Omega t + \hat{y}B_m \cos \Omega t$ to be measured in the x - y plane, as shown in Fig. 1(a). A pump light propagates

along the z axis. Furthermore, to induce the longitudinal parametric resonances, a modulation magnetic field $\mathbf{B}_1 = \hat{z}B_1 \cos \omega t$ is applied along the pump light. Although the spin evolution process appears complex in the laboratory frame, it can be significantly simplified in a rotating reference frame, which can help us gain a more intuitive understanding of the principle.

As shown in Fig. 1(a), the effective magnetic field in the rotating reference frame is $\tilde{\mathbf{B}} = \hat{y}B_m + \hat{z}(B_1 \cos \omega t - \Omega/\gamma)$. In this case, the experiment parameter setting of the scheme is the same as the typical longitudinal parametric resonance magnetometer [41–43]. When the modulation frequency coincides with the Larmor frequency of the effective magnetic field ω/γ , i.e., $\omega = \Omega$, the first-order parametric

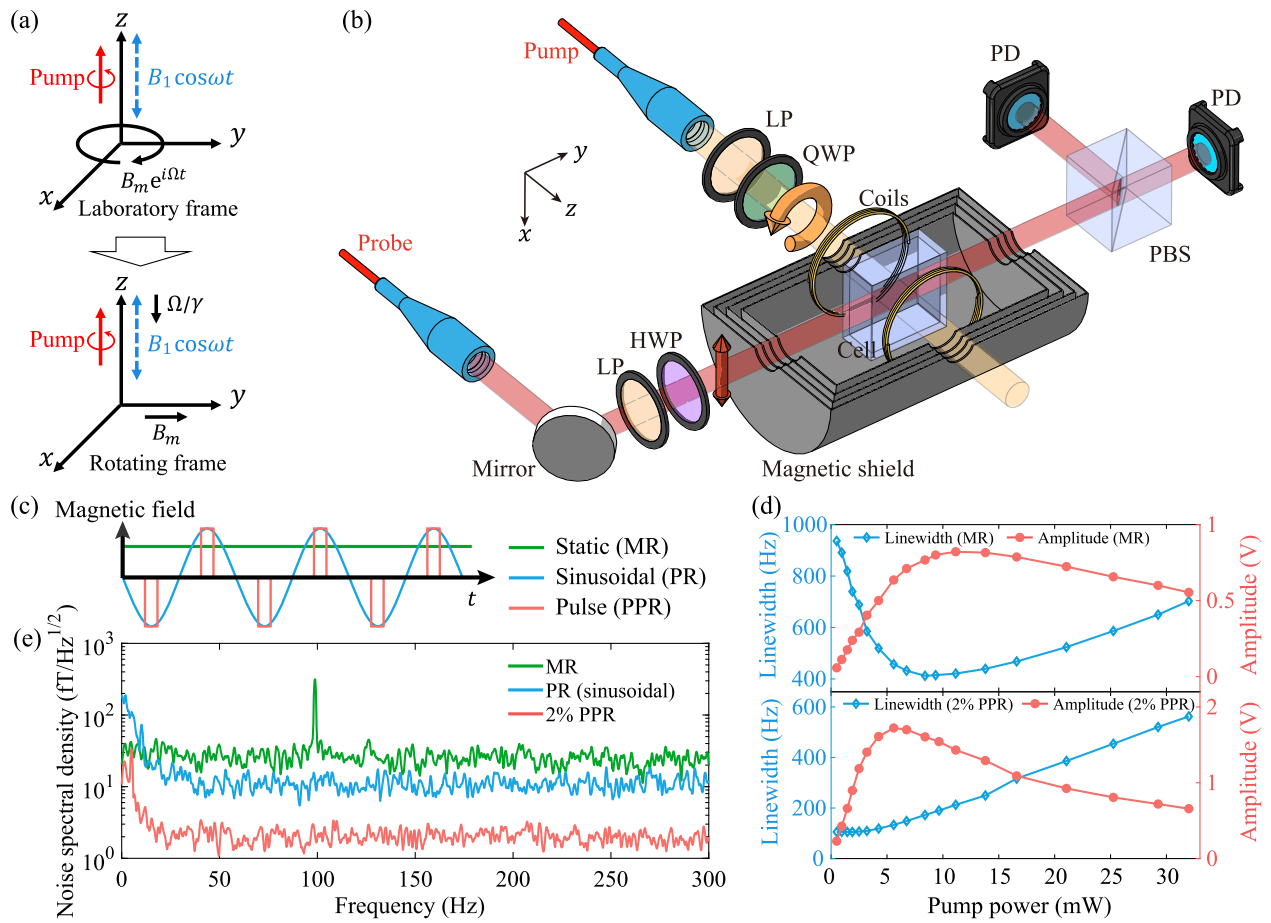


FIG. 1. The rf field detection scheme based on parametric resonances. (a) The experiment geometry is the same as the typical longitudinal parametric resonance magnetometer, where the transverse field B_m is measured by using the modulation field $B_1 \cos \omega t$. (b) Experimental setup of the rf magnetometer. A circularly polarized light propagating along the z axis is the pump light for polarizing the atoms. A linearly polarized light propagating along the y axis is used to detect the atomic spins. LP, linear polarized; HWP, half-wave plate; QWP, quarter-wave plate; PBS, polarizing beam splitter; PD, photodiode. (c) Schematic of three different waveforms of the modulation field for exciting magnetic resonances or parametric resonances. (d) The dependence of the linewidth and amplitude on the pump power in the case of MR scheme and pulsed PR (PPR) scheme. (e) The sensitivities of the rf magnetometer under three configurations. For the conventional MR scheme, the noise floor is around 25 fT/Hz^{1/2}. For the PR scheme employing a sinusoidal modulation field, its noise floor is improved to 12 fT/Hz^{1/2}. For a pulsed field with a duty cycle of 2%, a 12-times improvement is achieved in sensitivity, and the noise floor is up to 2 fT/Hz^{1/2}.

resonance emerges. For cases where the high-frequency condition $\omega \gg \Gamma = \Gamma_0 + R_{\text{OP}}$ is met, the approximate solution to Eq. (1) can be obtained. The first-order solution with the first harmonic is

$$P_y \approx -P_0 \frac{\gamma B_m}{\Gamma^2 + \delta^2} J_1^2 \left\{ \Gamma [\sin \Omega t + \sin(\Omega + 2\delta)t] + \delta [\cos \Omega t - \cos(\Omega + 2\delta)t] \right\}, \quad (2)$$

where $P_0 = sR_{\text{OP}}/\Gamma$ is the equilibrium electron spin polarization in the absence of magnetic fields, $\delta = \omega - \Omega$ is the frequency detuning, and $J_n = J_n(\gamma B_1/\omega)$ is the Bessel function of the order of n . The detailed derivations can be found in Supplemental Material [44]. When the resonance condition $\delta = 0$ is satisfied, the solution can be further simplified as

$$P_y \approx -P_0 \frac{\gamma B_m}{\Gamma} 2J_1^2 \sin \Omega t. \quad (3)$$

It shows that the spin polarization component P_y is sensitive to the strength of the rf field to be measured, which provides us another way to measure the rf field. The spin-relaxation rate Γ should generally be minimized for optimum performance.

Unlike conventional MR-based rf atomic magnetometers, where the bias field is present all the time and, thus, causes large SE relaxation, in our scheme the bias field is replaced with a time-varying modulation field to excite parametric resonances, which enables more possibilities to suppress the SE relaxation. Given the fact that the modulation field can be generalized to a periodical field with arbitrary waveform [37,45], the pulsed field is a better choice to excite the parametric resonances. For a pulsed field with a small duty cycle, there is no magnetic field interacting with the atoms most of the time. Although SE collisions still occur, they do not lead to SE relaxation during the time. So, the less duration of the modulation field present, the less SE relaxation would be induced by the field, as illustrated in Fig. 1(c). For a pulse modulation magnetic field $\mathbf{B}_1 = B_1 \eta(\cos \omega t)$, where

$$\eta(x) = \begin{cases} 0, & \text{if } |x| < \theta, \\ \text{sgn}(x - \theta), & \text{if } |x| > \theta \end{cases} \quad (4)$$

is a thresholding function to binarize the sinusoidal waveform with the threshold θ and $\text{sgn}(x - \theta)$ is the sign function, the duty cycle of the pulse modulation field can be derived as

$$d = 1 - \frac{4 \arcsin \theta}{2\pi}. \quad (5)$$

Since the SE relaxation vanishes when the modulation field equals zero, the spin relaxation induced by the pulsed field can be approximately expressed as $d\Gamma_{\text{SE}}$ [37,45,46], where Γ_{SE} represents the SE relaxation rate. A decrease in the duty

cycle corresponds a reduction in SE relaxation induced by the pulsed field.

Results—The experimental setup of the PR-based rf atomic magnetometer is illustrated in Fig. 1. A laser is sent through a linear polarizer and a quarter-wave plate to produce circularly polarized light for optically pumping the atoms. The pump light is tuned to the $D1$ resonance of Rb and propagates along the z direction. The ^{87}Rb vapor cell has a size of $6 \times 6 \times 3 \text{ mm}^3$ and is filled with 600 torr N_2 as a quenching and buffer gas. It is heated to 140°C and placed inside a cylindrical magnetic shield. The atomic spin polarization is detected using a linearly polarized light based on the optical rotation method. The probe light is red detuned by $\sim 60 \text{ GHz}$ away from the center of the Rb $D1$ line and is detected after the cell with a balanced photodetector to obtain the rotation of the light. The power of the probe light is $\sim 1 \text{ mW}$, and the diameter is $\sim 2 \text{ mm}$. A Helmholtz coil inside the shield generates the rf field to be measured.

We apply a 600 pT rf field with a frequency of 10 kHz as the rf field to be measured along the x direction to obtain the MR and the PR signal. To determine the optimal power of the pump light, we measure the dependence of the PR profile on the pump power. As a comparison, we further measure the linewidth and amplitude of the MR at the same pump power. As shown in Fig. 1(d), the MR linewidth initially decreases with increasing pump power due to light narrowing effects [40]. However, as the pump power continues to increase, the linewidth begins to increase due to the power broadening effects. In contrast, for the PR scheme employing a pulsed modulation field with a duty cycle of 2%, the linewidth remains nearly constant around 100 Hz as the pump power increases initially, indicating that the SE relaxation is almost eliminated. The PR-based rf atomic magnetometer achieves optimal sensitivity with lower pump power due to the suppressed SE relaxation, which is beneficial for the miniaturization of magnetometers.

Benefiting from the narrowed linewidth and enhanced signal amplitude, the PR-based rf magnetometer exhibits higher sensitivity compared with the MR scheme. Figure 1(e) shows the measured noise spectral density of the rf magnetometer in different configurations. The MR scheme demonstrates a typical noise floor of approximately $25 \text{ fT/Hz}^{1/2}$, which is consistent with other rf magnetometers utilizing a similar volume of atomic vapor cell. However, if we adopt a sinusoidal modulation field or a pulsed field with 2% duty cycle to induce the parametric resonances, the noise floor is improved to around 12 and $2 \text{ fT/Hz}^{1/2}$, respectively. The primary noise source of the magnetometer is the probe noise. After actively stabilizing the power of the probe light with an acousto-optic modulator, shot noise emerges as the dominant source of noise. Further decreasing the duty cycle of the pulsed field yields only a slight increase in sensitivity, as the SE relaxation is not the dominant factor in such cases.

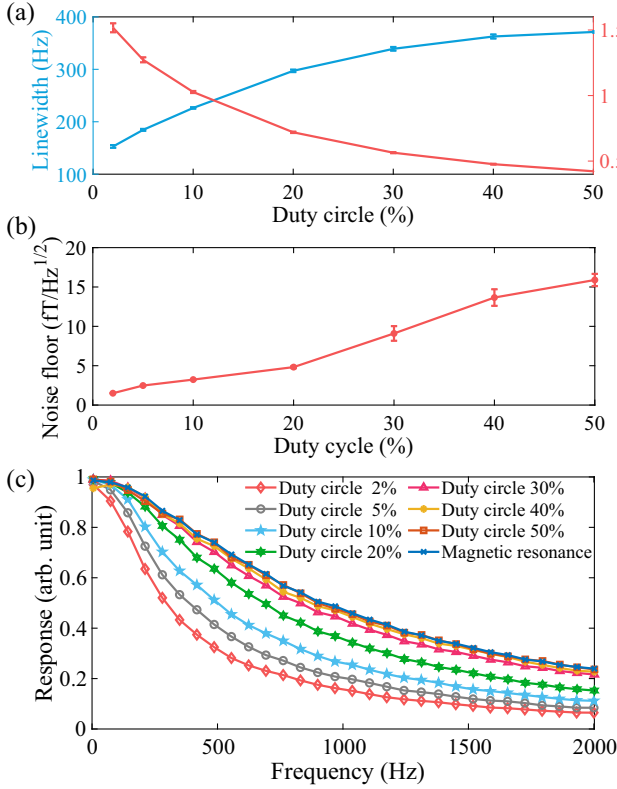


FIG. 2. The performance of the rf magnetometer based on PR scheme. (a) The dependence of the linewidth and amplitude of the PR signal on the duty cycle of the pulsed field. (b) The dependence of the noise floor on the duty cycle. (c) The frequency response of the rf atomic magnetometer under different magnetic field settings. A decrease in the duty cycle results in a narrower bandwidth due to the suppressed SE relaxation.

To further evaluate the PR-based rf magnetometer, experiments are conducted to examine the dependence of the PR profile on the duty cycle. The pump power is set to the optimal value of ~ 6 mW, which maximizes the ratio between the amplitude and linewidth of the PR profile, as illustrated in Fig. 1(d). It should be noted that, as the duty cycle varies, the amplitude of the pulsed field should be adjusted accordingly to maximize the PR signal. As demonstrated in Figs. 2(a) and 2(b), a decrease in duty cycle results in a narrower linewidth and larger signal amplitude, enhancing the sensitivity of the magnetometer. When the duty cycle is 50%, the noise floor reaches approximately 16 fT/Hz^{1/2}, comparable to the MR scheme. As the SE relaxation is suppressed in the PR scheme, the bandwidth of the rf magnetometer, determined by the spin relaxation rate, is also reduced. Figure 2(c) presents the frequency response of the magnetometer under different schemes. The frequency response is extracted by measuring the response to the rf field amplitude oscillating at varying frequencies while the rf frequency of the rf field is fixed at $\Omega = 10$ kHz. For the PPR scheme with a duty

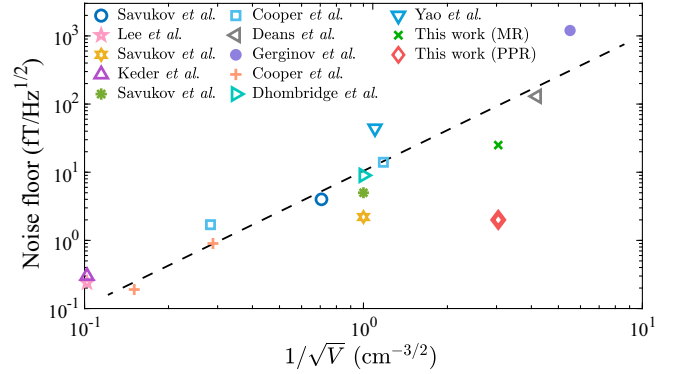


FIG. 3. The relationship between the noise floor of the rf atomic magnetometer and the effective sensing volume V is presented based on previous works. A linear relation can be roughly observed, as represented by the solid line. These results represented by the dots can be referred in Refs. [5–7,25,31,47–52].

cycle of 2%, the -3 dB bandwidth is ~ 290 Hz, whereas for the MR scheme, the bandwidth is ~ 920 Hz.

Discussion—Compared with the MR scheme, the PR scheme offers higher sensitivity due to the suppressed SE relaxation. As the fundamental theory $\delta B \propto V^{-1/2}$ [15,31] indicates, the sensitivity of atomic magnetometers can be improved by increasing the cell volume V to enhance signal strengths. Figure 3 shows the sensitivity-volume relationship based on previously developed MR-based rf atomic magnetometers. The cell volume is defined as the effective interaction volume between probe light and atoms. A roughly linear relation can be observed. If we implement the PPR atomic magnetometer with a larger cell, such as 100 cm³, the sensitivity could potentially improve by 30 times to 0.07 fT/Hz^{1/2}.

In addition to the high sensitivity of the PR scheme, it can also be phase sensitive, capable of measuring not only the rf field strength, but also its phase. The phase of the rf field can be determined by the amplitude of the spin response. Detailed derivations and discussions are provided in Supplemental Material [44]. Furthermore, the resonance condition of the PR scheme can be generalized to $n\omega = \Omega$, which implies the capability to measure not only the rf field oscillating at frequency Ω , but also its series of harmonics simultaneously. So, to measure a high-frequency rf field, we can just use a relatively low-frequency modulation field to excite the parametric resonance. These advantages can be particularly beneficial in MIT and NMR. If we further consider that there is a bias field $\hat{z}B_0$, the PR scheme remains effective, except that the resonance condition is modified to $n\omega = \Omega + \gamma B_0$. However, the presence of the bias field may result in an increased SE relaxation rate.

In contrast, the MR scheme relies on a static bias field, while the PR scheme employs a modulated field to induce the parametric resonances, which provides a bias-field-free method with higher sensitivity for rf field detection. It can be useful for some applications, such as the zero-field

NMR [14,16,17], which can provide ultrahigh-frequency resolution spectroscopy in comparison to the high-field NMR. For MRI using a flux transformer for decoupling the bias and gradient fields [21,22,48], the PR scheme can offer a higher signal-to-noise ratio (SNR) due to its higher sensitivity.

For the PR scheme using pulsed fields, a smaller duty cycle necessitates stronger modulation fields. In this way, the strong pulsed field might induce unexpected effects from the surroundings of the magnetometer. There are several ways to mitigate this issue, such as using well-designed magnetic field coils with little field leakage [53] or reducing the coil size to bring it closer to the cell. On the other hand, the modulation field generated by the coils can be advantageous in certain applications. For instance, in MIT using the MR-based rf atomic magnetometer, an rf field coil is typically needed to excite magnetization in the sample [9–12]. However, the magnetic field used to modulate the atoms in the PR scheme may also serve as the rf excitation field simultaneously, potentially eliminating the need for a separate rf excitation coil.

Conclusions—We have proposed a novel scheme based on parametric resonances for highly sensitive detection of rf fields. By using modulation field to excite parametric resonances instead of magnetic resonances, we realize an order of magnitude improvement in sensitivity of the rf magnetometer regarding to conventional magnetic-resonance-based rf magnetometer. A noise floor of $2 \text{ fT/Hz}^{1/2}$ within a small ^{87}Rb atomic vapor cell is achieved. As the experimental geometry of the parametric modulation scheme is almost the same as the MR-based scheme, the rf atomic magnetometer developed before can be easily transformed to the parametric-resonance scheme and achieve a higher sensitivity. Considering the wide applications of rf atomic magnetometers, the parametric resonance scheme is expected to make a significant improvement in these applications, such as higher-frequency resolution of NMR signals, higher SNR of MRI and MIT signals, etc.

Acknowledgments—This work is supported by the National Natural Science Foundation of China (Grants No. 62071012, No. 61571018, No. 61531003, and No. 91436210), the National Science Fund for Distinguished Young Scholars of China (Grant No. 61225003), and National Hi-Tech Research and Development (863) Program. T. W. acknowledges the support from the startup funding for young researchers of Peking University.

-
- [1] S. Tumanski, Induction coil sensors—a review, *Meas. Sci. Technol.* **18**, R31 (2007).
 [2] W. Buckel and R. Kleiner, *Superconductivity: Fundamentals and Applications*, Physics Textbook (Wiley, New York, 2008).
 [3] A. Fregosi, C. Gabbanini, S. Gozzini, L. Lenci, C. Marinelli, and A. Fioretti, Magnetic induction imaging with a

- cold-atom radio frequency magnetometer, *Appl. Phys. Lett.* **117**, 144102 (2020).
 [4] Y. Silani, J. Smits, I. Fescenko, M. W. Malone, A. F. McDowell, A. Jarmola, P. Kehayias, B. A. Richards, N. Mosavian, N. Ristoff, and V. M. Acosta, Nuclear quadrupole resonance spectroscopy with a femtotesla diamond magnetometer, *Sci. Adv.* **9**, eadh3189 (2023).
 [5] S.-K. Lee, K. L. Sauer, S. J. Seltzer, O. Alem, and M. V. Romalis, Subfemtotesla radio-frequency atomic magnetometer for detection of nuclear quadrupole resonance, *Appl. Phys. Lett.* **89**, 214106 (2006).
 [6] D. A. Keder, D. W. Prescott, A. W. Conovaloff, and K. L. Sauer, An unshielded radio-frequency atomic magnetometer with sub-femtotesla sensitivity, *AIP Adv.* **4**, 127159 (2014).
 [7] R. J. Cooper, D. W. Prescott, K. L. Sauer, N. Dural, and M. V. Romalis, Intrinsic radio-frequency gradiometer, *Phys. Rev. A* **106**, 053113 (2022).
 [8] C. Deans, L. Marmugi, S. Hussain, and F. Renzoni, Electromagnetic induction imaging with a radio-frequency atomic magnetometer, *Appl. Phys. Lett.* **108**, 103503 (2016).
 [9] A. Wickenbrock, N. Leefer, J. W. Blanchard, and D. Budker, Eddy current imaging with an atomic radio-frequency magnetometer, *Appl. Phys. Lett.* **108**, 183507 (2016).
 [10] P. Bevington, R. Gartman, W. Chalupczak, C. Deans, L. Marmugi, and F. Renzoni, Non-destructive structural imaging of steelwork with atomic magnetometers, *Appl. Phys. Lett.* **113**, 063503 (2018).
 [11] K. Jensen, M. Zugenmaier, J. Arnbak, H. Stærkind, M. V. Balabas, and E. S. Polzik, Detection of low-conductivity objects using eddy current measurements with an optical magnetometer, *Phys. Rev. Res.* **1**, 033087 (2019).
 [12] C. Deans, Y. Cohen, H. Yao, B. Maddox, A. Vigilante, and F. Renzoni, Electromagnetic induction imaging with a scanning radio frequency atomic magnetometer, *Appl. Phys. Lett.* **119**, 014001 (2021).
 [13] W. Zheng, H. Wang, R. Schmiege, A. Oesterle, and E. S. Polzik, Entanglement-enhanced magnetic induction tomography, *Phys. Rev. Lett.* **130**, 203602 (2023).
 [14] D. P. Weitekamp, A. Bielecki, D. Zax, K. Zilm, and A. Pines, Zero-field nuclear magnetic resonance, *Phys. Rev. Lett.* **50**, 1807 (1983).
 [15] I. M. Savukov and M. V. Romalis, NMR detection with an atomic magnetometer, *Phys. Rev. Lett.* **94**, 123001 (2005).
 [16] M. C. D. Tayler, T. Theis, T. F. Sjolander, J. W. Blanchard, A. Kentner, S. Pustelny, A. Pines, and D. Budker, Invited Review Article: Instrumentation for nuclear magnetic resonance in zero and ultralow magnetic field, *Rev. Sci. Instrum.* **88**, 091101 (2017).
 [17] M. Jiang, T. Wu, J. W. Blanchard, G. Feng, X. Peng, and D. Budker, Experimental benchmarking of quantum control in zero-field nuclear magnetic resonance, *Sci. Adv.* **4**, eaar6327 (2018).
 [18] S. Alciček, P. Put, V. Kontul, and S. Pustelny, Zero-field NMR J-spectroscopy of organophosphorus compounds, *J. Phys. Chem. Lett.* **12**, 787 (2021).
 [19] S. Xu, V. V. Yashchuk, M. H. Donaldson, S. M. Rochester, D. Budker, and A. Pines, Magnetic resonance imaging with an optical atomic magnetometer, *Proc. Natl. Acad. Sci. U.S.A.* **103**, 12668 (2006).

- [20] V. S. Zotev, A. N. Matlashov, P. L. Volegov, I. M. Savukov, M. A. Espy, J. C. Mosher, J. J. Gomez, and R. H. Kraus, Microtesla MRI of the human brain combined with MEG, *J. Magn. Reson.* **194**, 115 (2008).
- [21] I. Savukov, V. Zotev, P. Volegov, M. Espy, A. Matlashov, J. Gomez, and R. Kraus, MRI with an atomic magnetometer suitable for practical imaging applications, *J. Magn. Reson.* **199**, 188 (2009).
- [22] I. Savukov and T. Karaulanov, Magnetic-resonance imaging of the human brain with an atomic magnetometer, *Appl. Phys. Lett.* **103**, 043703 (2013).
- [23] G. Bevilacqua, V. Biancalana, Y. Dancheva, and A. Vigilante, Sub-millimetric ultra-low-field MRI detected *in situ* by a dressed atomic magnetometer, *Appl. Phys. Lett.* **115**, 174102 (2019).
- [24] A. Garroway, M. Buess, J. Miller, B. Suits, A. Hibbs, G. Barrall, R. Matthews, and L. Burnett, Remote sensing by nuclear quadrupole resonance, *IEEE T. Geosci. Remote* **39**, 1108 (2001).
- [25] R. J. Cooper, D. W. Prescott, P. Matz, K. L. Sauer, N. Dural, M. V. Romalis, E. L. Foley, T. W. Kornack, M. Monti, and J. Okamitsu, Atomic magnetometer multisensor array for rf interference mitigation and unshielded detection of nuclear quadrupole resonance, *Phys. Rev. Appl.* **6**, 064014 (2016).
- [26] D. R. Quiroz, R. J. Cooper, E. L. Foley, T. W. Kornack, G. J. Lee, and K. L. Sauer, Interleaved NQR detection using atomic magnetometers, *J. Magn. Reson.* **343**, 107288 (2022).
- [27] A. Weis, G. Bison, and Z. D. Grujić, Magnetic resonance based atomic magnetometers, in *High Sensitivity Magnetometers*, edited by A. Grosz, M. J. Haji-Sheikh, and S. C. Mukhopadhyay (Springer, New York, 2017), pp. 361–424.
- [28] W. Happer and A. C. Tam, Effect of rapid spin exchange on the magnetic-resonance spectrum of alkali vapors, *Phys. Rev. A* **16**, 1877 (1977).
- [29] I. M. Savukov and M. V. Romalis, Effects of spin-exchange collisions in a high-density alkali-metal vapor in low magnetic fields, *Phys. Rev. A* **71**, 023405 (2005).
- [30] W. Xiao, T. Wu, X. Peng, and H. Guo, Atomic spin-exchange collisions in magnetic fields, *Phys. Rev. A* **103**, 043116 (2021).
- [31] I. Savukov, T. Karaulanov, and M. G. Boshier, Ultra-sensitive high-density Rb-87 radio-frequency magnetometer, *Appl. Phys. Lett.* **104**, 023504 (2014).
- [32] M. Lipka, A. Sierant, C. Troullinou, and M. W. Mitchell, Multiparameter quantum sensing and magnetic communication with a hybrid dc and rf optically pumped magnetometer, *Phys. Rev. Appl.* **21**, 034054 (2024).
- [33] J. C. Allred, R. N. Lyman, T. W. Kornack, and M. V. Romalis, High-sensitivity atomic magnetometer unaffected by spin-exchange relaxation, *Phys. Rev. Lett.* **89**, 130801 (2002).
- [34] I. Kominis, T. Kornack, J. Allred, and M. V. Romalis, A subfemtotesla multichannel atomic magnetometer, *Nature (London)* **422**, 596 (2003).
- [35] M. P. Ledbetter, V. M. Acosta, S. M. Rochester, D. Budker, S. Pustelny, and V. V. Yashchuk, Detection of radio-frequency magnetic fields using nonlinear magneto-optical rotation, *Phys. Rev. A* **75**, 023405 (2007).
- [36] W. Chalupczak, R. M. Godun, S. Pustelny, and W. Gawlik, Room temperature femtotesla radio-frequency atomic magnetometer, *Appl. Phys. Lett.* **100**, 242401 (2012).
- [37] A. Korver, R. Wyllie, B. Lancor, and T. G. Walker, Suppression of spin-exchange relaxation using pulsed parametric resonance, *Phys. Rev. Lett.* **111**, 043002 (2013).
- [38] S. Appelt, A. B. Baranga, A. R. Young, and W. Happer, Light narrowing of rubidium magnetic-resonance lines in high-pressure optical-pumping cells, *Phys. Rev. A* **59**, 2078 (1999).
- [39] T. Scholtes, S. Pustelny, S. Fritzsche, V. Schultze, R. Stolz, and H.-G. Meyer, Suppression of spin-exchange relaxation in tilted magnetic fields within the geophysical range, *Phys. Rev. A* **94**, 013403 (2016).
- [40] Y. Fu, X. Liu, and J. Yuan, Light narrowing of cesium magnetic-resonance lines in a radio-frequency atomic magnetometer, *AIP Adv.* **9**, 015304 (2019).
- [41] C. Cohen-Tannoudji, J. Dupont-Roc, S. Haroche, and F. Laloë, Diverses résonances de croisement de niveaux sur des atomes pompés optiquement en champ nul. I. théorie, *Rev. Phys. Appl.* **5**, 95 (1970).
- [42] Z. Li, R. T. Wakai, and T. G. Walker, Parametric modulation of an atomic magnetometer, *Appl. Phys. Lett.* **89**, 134105 (2006).
- [43] Z. Ding, J. Yuan, G. Lu, Y. Li, and X. Long, Three-axis atomic magnetometer employing longitudinal field modulation, *IEEE Photonics J.* **9**, 1 (2017).
- [44] See Supplemental Material at <http://link.aps.org/supplemental/10.1103/PhysRevLett.133.093201> for the detailed derivation of the equations that describing the spin response to the rf field in the case of the PR-based rf field detection scheme.
- [45] G. Bevilacqua, V. Biancalana, Y. Dancheva, and L. Moi, Larmor frequency dressing by a nonharmonic transverse magnetic field, *Phys. Rev. A* **85**, 042510 (2012).
- [46] M. E. Limes, D. Sheng, and M. V. Romalis, $^3\text{He} - ^{129}\text{Xe}$ comagnetometry using ^{87}Rb detection and decoupling, *Phys. Rev. Lett.* **120**, 033401 (2018).
- [47] I. M. Savukov, S. J. Seltzer, M. V. Romalis, and K. L. Sauer, Tunable atomic magnetometer for detection of radio-frequency magnetic fields, *Phys. Rev. Lett.* **95**, 063004 (2005).
- [48] I. Savukov and T. Karaulanov, Anatomical MRI with an atomic magnetometer, *J. Magn. Reson.* **231**, 39 (2013).
- [49] V. Gerginov, F. C. S. da Silva, A. Hati, and C. Nelson, An atomic sensor for direct detection of weak microwave signals, *IEEE Trans. Microwave Theory Tech.* **67**, 3485 (2019).
- [50] C. Deans, L. Marmugi, and F. Renzoni, Sub-picotesla widely tunable atomic magnetometer operating at room-temperature in unshielded environments, *Rev. Sci. Instrum.* **89**, 083111 (2018).
- [51] J. E. Dhombridge, N. R. Claussen, J. Iivanainen, and P. D. D. Schwindt, High-sensitivity rf detection using an optically pumped comagnetometer based on natural-abundance rubidium with active ambient-field cancellation, *Phys. Rev. Appl.* **18**, 044052 (2022).
- [52] H. Yao, B. Maddox, and F. Renzoni, Neural network-aided optimisation of a radio-frequency atomic magnetometer, *Opt. Express* **31**, 27287 (2023).
- [53] N. V. Nardelli, S. P. Krzyzewski, and S. A. Knappe, Reducing crosstalk in optically-pumped magnetometer arrays, *Phys. Med. Biol.* **64**, 21NT03 (2019).